

## Prestressed fracture specimen for delamination testing of composites

ANDRÁS SZEKRÉNYES

*Department of Applied Mechanics, Budapest University of Technology and Economics, H-1521  
Budapest, P.O. Box 11, Hungary  
(E-mail: szeki@mm.bme.hu)*

Received 13 June 2005; accepted 3 February 2006

**Abstract.** The prestressed end-notched flexure fracture specimen is developed in the present work, which combines the traditional double-cantilever beam and the end-notched flexure specimens in a very simple way. The most important features of the new beam-like specimen are that it is able to provide any combination of the modes I and II strain energy release rates and it may be performed by using a simple three-point bending fixture. The mode-I part of the strain energy release rate is fixed by inserting a steel roller, which causes a fixed crack opening displacement. The mode-II part of the energy release rate is provided by the external load. A simple closed-form solution using beam theory is developed for the energy release rates of the new configuration. The applicability and the limitations of the novel configuration are demonstrated using unidirectional glass/polyester composite specimens. If only propagation onset is involved then the prestressed end-notched flexure specimen can be used to obtain the fracture criterion of transparent composite materials in a very simple way.

**Key words:** Beam theory, double-cantilever beam, end-notched flexure, interlaminar fracture, three-point bending, variable mode-mixity.

### 1. Introduction

The delamination testing of composite materials plays very important role in the practical life. To determine the fracture criterion the strain energy release rate (SERR) of the material should be determined under different combinations of the modes I and II loading. In the case of the pure modes I and II there are different configurations, which are relatively easy to perform. The double-cantilever beam (DCB) is a standard tool (ASTM D5528, ISO/DIS 15024) to measure the mode-I toughness of composites (Williams, 1989; Olsson, 1992; Ozdil and Carlsson, 1999a; Morais et al., 2002). For mode-II testing six specimens are available: the end-notched flexure (ENF) (Carlsson et al., 1986; Wang and Williams, 1992; Wang and Qiao, 2004), the stabilized end-notched flexure (SENF) (e.g. Davies et al., 1996), the end-loaded split (ELS) (Davies et al., 1996; Wang and Vu-Khanh 1996), the 4-point bend end-notched flexure (4ENF) (Schuecker and Davidson, 2000; Davies et al., 2005), the over-notched flexure (ONF) (Wang et al., 2003; Szekrényes and Uj, 2005) and the tapered end-notched flexure (TENF) coupons (Edde et al., 1995; Qiao et al., 2003b, Wang and Qiao 2003). Each configuration has advantages and relative drawbacks as it has been highlighted for example by Szekrényes and Uj (2005). The mixed-mode I/II is the combination of the pure modes I and II. A mixed-mode I/II configuration, which satisfies the following requirements, would be preferable:

- Able to produce any combination of the modes I and II, i.e. able to vary the mode-ratio within wide ranges.
- Requires a simple experimental equipment.
- The experimental data is easy to reduce.
- Involves a simple analytical and numerical solution.
- Can be applied for a wide variety of material pairs.

It has been shown that numerous excellent mixed-mode configurations exist, but none of these satisfies the above requirements (Reeder and Crews, 1990; Davidson and Sundararaman, 1996). The asymmetric DCB (ADCB) specimen was proposed by Bradley and Cohen (1985). However, this involved loading the arms of the specimen with two different loads, which is possible by using a complex loading system. Hashemi et al. (1987) developed the variable mixed-mode (VMM) test. Due to certain complications (e.g., the mode ratio changes with the crack length) neither this one became the optimal solution. The cracked-lap shear (CLS) (Lai et al., 1996; Rhee and Chi, 2001) specimen was also an attempt to construct a many-sided specimen. Due to its significant disadvantages (large rotations at the crack tip, complex analysis, etc.) it is used only in few cases. The single-cantilever beam (SCB) (Hashemi et al., 1990a, b; Szekrényes and Uj, 2004), the single-leg bending (SLB) (Yoon and Hong, 1990a; Davidson and Sundararaman, 1996; Szekrényes and Uj, 2004), and the mixed-mode flexure (MMF) (Korjakin et al., 1998) specimens are able to produce only a constant mixed-mode ratio. However, varying the thickness ratio of the upper and lower specimen arms of the DCB (which is an ESIS TC4 standard) (Sundararaman and Davidson, 1997; ESIS, 2000), ENF (Sundararaman and Davidson, 1998), SCB (Hashemi et al., 1990b), and SLB (Davidson and Sundararaman, 1996) specimens and applying different material pairs it is possible to produce different mode ratios. In this case different specimen geometry is necessary and furthermore, geometrical nonlinearities may also arise.

The most universal mixed-mode I/II tool is the mixed-mode bending (MMB, ASTM D6671-01) specimen, which was developed by Crews and Reeder (1988) and Reeder and Crews (1990). It is able to produce any mode-ratio, however it has many drawbacks. First of all it requires a complex fixture and bonded steel hinged tabs. Apart from that a beam theory-based reduction technique was recommended, which is reliable in the case of unidirectional composites, but questionable in the case of multidirectional laminates. Later, an experimental compliance calibration (CC) was developed for data reduction (e.g., Ducept et al., 1999). In addition, unstable crack propagation may occur if the fracture is mode-II dominated. Later, the MMB was redesigned in order to reduce the nonlinear effects and take the weight of the lever into account (Reeder and Crews, 1991; Reeder, 1992, 2000). A very large amount of experimental work was performed using the MMB specimen (Ducept et al., 1997, 1999, 2000; Asp et al., 1998, Chen et al., 1999; Ozdil and Carlsson, 1999b; Kim and Mayer, 2003). It should be mentioned that the fracture envelope obtained by the updated test rig was quite different than that of the original apparatus (Reeder and Crews, 1991).

Therefore, the development of the different setups is still in progress nowadays. The single leg four-point bend (SLFPB) test was developed by Tracy et al. (2003). The so-called over-leg bending (OLB) is the modified version of the traditional

SLB one (Szekrényes and Uj, 2006b). Both are suitable for crack propagation measurement; however these specimens do not overcome the MMB specimen. Ifju et al. (2002) and Chen et al. (2003) developed three new mixed-mode I/II setups for the testing of stitched composites. The main advantage of these setups is that the fiber micro-buckling may be eliminated. Although the energy release rate can be determined at any mode ratio, the setups require special grips and a clamping fixture. The next step was done by Sørensen et al. (2004), who updated the ADCB configuration by loading the specimen by different moments, so the DCB specimen loaded by uneven bending moments (DCB-UBM) was developed. In some points of view this method overcomes the MMB test, i.e. it promotes stable crack propagation at any mode ratio, and the mixed-mode cohesive laws (3D plot of the fracture resistance versus the crack opening and shearing displacements) can be determined. However, this is very time-consuming. On the other hand, the test requires a complex fixture, bonded steel tabs and the measured data is again can be reduced only by a beam theory solution. So, despite the large number of the developed beam-like fracture specimens there is not an optimal solution.

Apart from the beam-like specimens there are also other possibilities to determine the fracture criterion of composite materials. The edge delaminated tension (EDT) test was discussed in detail by Raju et. al (1988), the drawbacks of the test were summarized by Reeder and Crews (1990). The Arcan-type fixture was developed in 1978 (Arcan et al., 1978). Among others Yoon and Hong (1990b) applied the Arcan test to determine the fracture criterion for graphite/epoxy laminates. Later Rikards et al. (1998) proposed the compact tension shear specimen (CTS), which is eventually based on the Arcan test. Although the Arcan test covers all the mixed-mode ratios including the pure mode-I to mode-II, the results can only be obtained by a numerical (finite element) analysis, which involves the singularity at the crack tip. On the other hand the test uses a complex loading fixture.

This work presents a novel configuration for mixed-mode I/II interlaminar fracture testing. The prestressed end-notched flexure (PENF) coupon exhibits several advantages in comparison with the existing mixed-mode I/II specimens. The test may be performed in a three-point bending setup, does not requires bonded steel tabs and any mode ratio can be obtained at the crack length of interest. A relative drawback of the test is that the mode ratio significantly changes with the crack length and the applied load, and the mode ratio can be determined only after the experiment has been performed. Thus, the advantages of the PENF specimen over the previously developed universal tests can be exploited if only crack propagation onset (initiation) is involved.

## **2. The prestressed end-notched flexure specimen**

### **2.1. ENERGY RELEASE RATE AND MODE RATIO**

The PENF specimen simply combines the traditional DCB and ENF coupons. As it is shown in Figure 1 the crack opening displacement (COD), and so the mode-I part of the problem is fixed by inserting a steel roller at the delamination plane. To determine the strain energy release rate of the PENF specimen we apply Williams' global mode decomposition method (Williams, 1988; Ducept et al., 1999), which gives the following expressions for the modes I and II energy release rates:

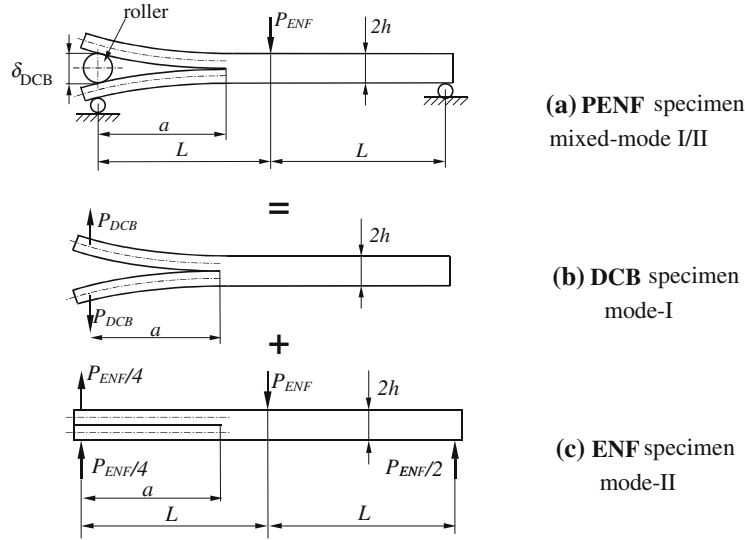


Figure 1. The mixed-mode I/II PNF specimen (a) as the superposition of the DCB (b) and ENF (c) specimens.

$$G_I = \frac{12M_I^2}{b^2h^3E_{11}}, \quad (1)$$

$$G_{II} = \frac{9M_{II}^2}{b^2h^3E_{11}}, \quad (2)$$

where  $b$  is the width of the specimen,  $h$  is half of the thickness and  $E_{11}$  is the flexural modulus of the specimen, furthermore:

$$M_I = (M_1 - M_2)/2, \quad M_{II} = (M_1 + M_2)/2, \quad (3)$$

where  $M_1$  and  $M_2$  are bending moments at the upper and lower arms at the crack tip. Based on Figure 1a–c we treat the PNF specimen as the superposition of the DCB and ENF specimens. So we may write:

$$M_1 = \left( P_{DCB} + \frac{P_{ENF}}{4} \right) a, \quad M_2 = \left( -P_{DCB} + \frac{P_{ENF}}{4} \right) a. \quad (4)$$

Incorporating Equation (3) we obtain:

$$M_I = P_{DCB}a, \quad M_{II} = \frac{P_{ENF}}{4}a. \quad (5)$$

Using a three-point bending setup the external force is equal to  $P_{ENF}$ . To calculate the force  $P_{DCB}$ , which causes the fixed COD ( $\delta_{DCB}$ ), we need the compliance of the DCB specimen, which (using simple beam theory) is (Williams, 1989; Olsson, 1992):

$$C_{DCB} = \frac{8a^3}{bh^3E_{11}} = \frac{\delta_{DCB}}{P_{DCB}}. \quad (6)$$

Rearranging Equation (6) we obtain:

$$P_{\text{DCB}} = \frac{bh^3 E_{11} \delta_{\text{DCB}}}{8a^3}. \quad (7)$$

Combining Equations (7) and (5) with Equations (1) and (2) we obtain the SERRs of the PENF specimen:

$$G_{\text{I}} = \frac{3h^3 E_{11} \delta_{\text{DCB}}^2}{16a^4}, \quad (8)$$

$$G_{\text{II}} = \frac{9P_{\text{ENF}}^2 a^2}{16b^2 h^3 E_{11}}. \quad (9)$$

The mode ratio by combining Equations (8) and (9) is:

$$\frac{G_{\text{I}}}{G_{\text{II}}} = \frac{b^2 E_{11}^2}{3} \left(\frac{h}{a}\right)^6 \left(\frac{\delta_{\text{DCB}}}{P_{\text{ENF}}}\right)^2. \quad (10)$$

If the COD is fixed then – in accordance with Equation (10) – the mode-ratio depends on the applied load  $P_{\text{ENF}}$  and the crack length  $a$ .

It has been shown that the result of Euler–Bernoulli beam theory for the compliance and SERRs of the common specimens can be significantly improved (Williams, 1989; Olsson, 1992; Wang and Qiao, 2004; Szekrényes and Uj, 2004, 2006a; Szekrényes, 2005). In the following we derive a refined solution. The expressions incorporate the Winkler–Pasternak-type elastic foundation (Szekrényes, 2005), transverse shear analysis (Ozdil et al., 1998), Saint-Venant effect (Olsson, 1992) and crack tip shear deformation (Wang and Qiao, 2004). In our last works Williams’ global method was improved with the mentioned effects (Szekrényes, 2005; Szekrényes and Uj, 2006a):

$$G_{\text{I}} = \frac{M_{\text{I}}^2 (12 + f_{\text{W2}} + f_{\text{T}} + f_{\text{SV}})}{b^2 h^3 E_{11}}, \quad (11)$$

$$G_{\text{II}} = \frac{M_{\text{II}}^2 (9 + f_{\text{SH2}})}{b^2 h^3 E_{11}}, \quad (12)$$

where

$$f_{\text{W2}} = 10.14 \left(\frac{h}{a}\right) \left(\frac{E_{11}}{E_{33}}\right)^{1/4} + 8.58 \left(\frac{h}{a}\right)^2 \left(\frac{E_{11}}{E_{33}}\right)^{1/2}, \quad (13)$$

$$f_{\text{T}} = \frac{1}{k} \left(\frac{h}{a}\right)^2 \left(\frac{E_{11}}{G_{13}}\right), \quad (14)$$

$$f_{\text{SV}} = \frac{12}{\pi} \left(\frac{h}{a}\right) \left(\frac{E_{11}}{G_{13}}\right)^{1/2}, \quad (15)$$

$$f_{\text{SH2}} = 1.96 \left( \frac{h}{a} \right) \left( \frac{E_{11}}{G_{13}} \right)^{1/2} + 0.43 \left( \frac{h}{a} \right)^2 \left( \frac{E_{11}}{G_{13}} \right), \quad (16)$$

where  $f_{\text{W2}}$  is the correction from the Winkler–Pasternak foundation,  $f_{\text{T}}$  is the effect of transverse shear,  $f_{\text{SV}}$  is the correction from Saint-Venant effect,  $f_{\text{SH2}}$  is the effect of crack tip shear deformation and  $k = 5/6$  is the shear correction factor. The improved compliance expression of the DCB specimen is (Szekrényes, 2005):

$$C^{\text{DCB}} = \frac{8a^3}{bh^3E_{11}} + \frac{2a^3}{bh^3E_{11}}(f_{\text{W1}} + f_{\text{T}} + f_{\text{SV}}), \quad (17)$$

where  $f_{\text{W1}}$  is the effect of the Winkler–Pasternak elastic foundation:

$$f_{\text{W1}} = 5.07 \left( \frac{h}{a} \right) \left( \frac{E_{11}}{E_{33}} \right)^{1/4} + 8.58 \left( \frac{h}{a} \right)^2 \left( \frac{E_{11}}{E_{33}} \right)^{1/2} + 2.08 \left( \frac{h}{a} \right)^3 \left( \frac{E_{11}}{E_{33}} \right)^{3/4}. \quad (18)$$

From Equation (17) the force, which arises in the DCB specimen, is:

$$P_{\text{DCB}} = \frac{bh^3E_{11}\delta_{\text{DCB}}}{8a^3} \frac{1}{1 + (f_{\text{W1}} + f_{\text{T}} + f_{\text{SV}})/4}. \quad (19)$$

Combining Equations (19) and (5) with Equations (11) and (12) leads to the following expressions:

$$G_{\text{I}} = \frac{h^3E_{11}\delta_{\text{DCB}}^2}{64a^4} \frac{[12 + f_{\text{W2}} + f_{\text{T}} + f_{\text{SV}}]}{[1 + (f_{\text{W1}} + f_{\text{T}} + f_{\text{SV}})/4]^2}, \quad (20)$$

$$G_{\text{II}} = \frac{P_{\text{ENF}}^2 a^2}{16b^2 h^3 E_{11}} [9 + f_{\text{SH2}}]. \quad (21)$$

In this case the mode ratio is:

$$\frac{G_{\text{I}}}{G_{\text{II}}} = \frac{b^2 E_{11}^2}{4} \left( \frac{h}{a} \right)^6 \left( \frac{\delta_{\text{DCB}}}{P_{\text{ENF}}} \right)^2 \frac{(12 + f_{\text{W2}} + f_{\text{T}} + f_{\text{SV}})}{[1 + (f_{\text{W1}} + f_{\text{T}} + f_{\text{SV}})/4]^2} \frac{1}{(9 + f_{\text{SH2}})}. \quad (22)$$

Consequently, the mode ratio (or the mode-I SERR) can be controlled by varying the diameter of the steel roller. If we increase the diameter, then it is expected that the applied load required for crack initiation,  $P_{\text{ENF}}$  will decrease. If we suppose to perform crack propagation test and the crack length approaches to infinity, the mode-I SERR will subsequently decay and it will tend to a pure mode-II problem. Hence, the mode ratio will also change as the crack propagates.

Figure 2a and b shows, the variation of the mode ratio against the normalized applied load and the crack length. These results were calculated using improved beam theory (IBT) (Equation (22),  $b = 20$  mm,  $h = 3$  mm,  $L = 75$  mm,  $E_{11} = 33$  GPa,  $E_{33} = 7.2$  GPa,  $G_{13} = 3$  GPa) and are strictly to demonstrate the changes in the mode ratio of the present E-glass/polyester material at given crack openings ( $\delta_{\text{DCB}} = 0.5$  and 3.0 mm in Figure 2a, and  $\delta_{\text{DCB}} = 0.5$  and 4.0 mm in Figure 2b). The maximal values of the load ( $P_{\text{max}}$ ) and crack length ( $a_{\text{max}}$ ) are chosen arbitrarily. It is important to identify the crack initiation accurately. On the one hand, if we measure the critical applied load inaccurately, then the mode-II SERR (and so the mode ratio) will

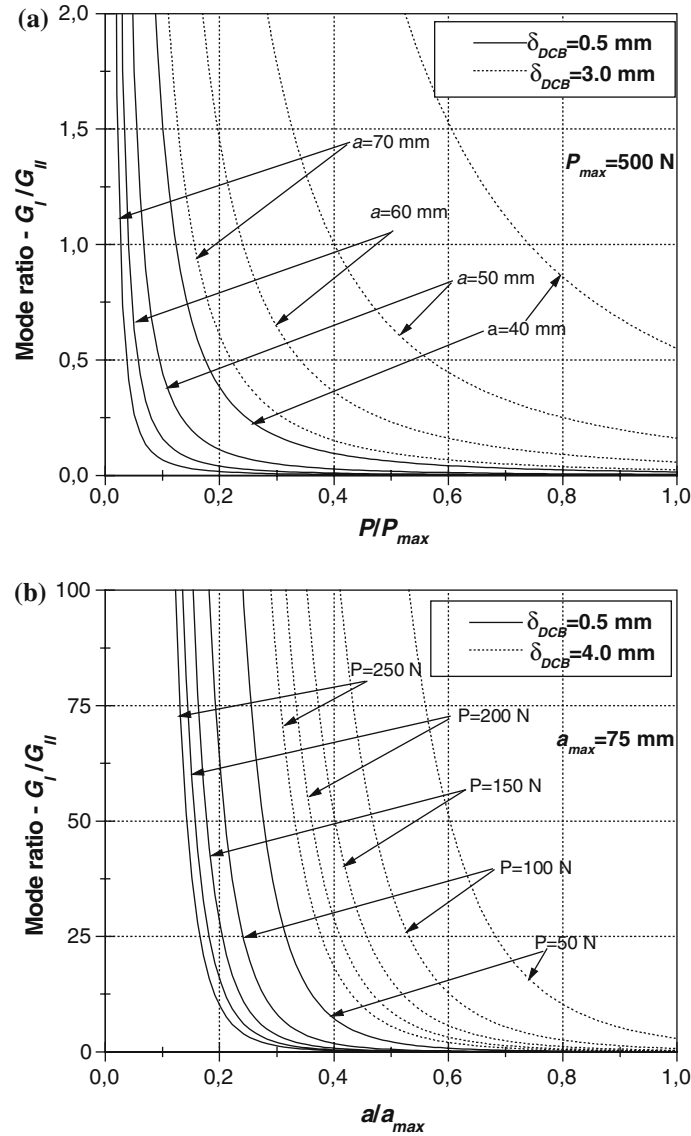


Figure 2. Variation of the mode-ratio in the PENF specimen as the function of the applied load (a) and the crack length (b).

change. On the other hand, after crack initiation some increase in the crack length may be expected, which also causes changes in the mode ratio. It is also important to note that the mode ratio depends on the elastic properties of the material (see Equation (22)). Table 1 addresses this issue including three material types: the present glass/polyester material (with low flexural modulus,  $E_{11}$ ), an isotropic one and a carbon/PEEK composite (with high flexural modulus, investigated by Hashemi et al., 1990a). The first block demonstrates the changes in the mode ratio with the load at a given crack length ( $a = 55$  mm) including given crack openings ( $\delta_{DCB} = 2$  and  $\delta_{DCB} = 3$  mm). The mode ratio drastically changes, especially in the case of the carbon/PEEK material, while the difference between the glass/polyester and the isotropic material is not significant. The second block of Table 1 demonstrates the

Table 1. The effect of elastic properties on the mode ratio of the PENF specimen.

	Glass/polyester			Isotropic			Carbon/PEEK		
$P$ (N)	50	100	150	50	100	150	50	100	150
$a = 55$ mm	$G_I/G_{II}$			$G_I/G_{II}$			$G_I/G_{II}$		
$\delta = 2$ mm	4.19	1.05	0.47	5.06	1.27	0.56	49.9	12.5	5.55
$\delta = 3$ mm	9.44	2.36	1.05	11.4	2.85	1.27	112.4	28.1	12.5
$a$ (mm)	50	60	70	50	60	70	50	60	70
$P = 150$ N	$G_I/G_{II}$			$G_I/G_{II}$			$G_I/G_{II}$		
$\delta = 2$ mm	0.78	0.29	0.12	0.97	0.34	0.14	9.31	3.45	1.47
$\delta = 3$ mm	1.78	0.64	0.27	2.19	0.76	0.31	20.9	7.76	3.31

$h = 3.05$  mm,  $b = 20$  mm, Glass/polyester:  $E_{11} = 33$  GPa,  $E_{33} = 7.2$  GPa,  $G_{13} = 3$  GPa, Isotropic:  $E_{11} = 33$  GPa,  $E_{33} = 33$  GPa,  $G_{13} = 12.7$  GPa, Carbon/PEEK:  $E_{11} = 124$  GPa,  $E_{33} = 10$  GPa,  $G_{13} = 5$  GPa.

values of the mode ratio by varying the crack length at a given load value ( $P = 150$  N). These results indicate the same trends as it was found in the first block of Table 1, i.e. the sensitivity of the mode ratio to the crack length and applied load requires the accurate determination of these quantities. The accurate determination of the critical load and the observation of the crack initiation are relatively easy tasks in the present material due to its transparency.

## 2.2. CRACK STABILITY

The stability of the PENF system can be investigated based on the derivative of the SERR with respect to the crack length, i.e.,  $dG_{I/II}/da$ . If this is zero or negative then stable crack growth may be expected. We consider the case of fixed grip conditions (Carlsson et al., 1986). Furthermore, only the results of the Euler–Bernoulli beam theory are considered. The derivative of the energy release rate may be written as:

$$\frac{dG_{I/II}}{da} = \frac{dG_I}{da} + \frac{dG_{II}}{da}. \quad (23)$$

Differentiating Equation (8) we obtain:

$$\frac{dG_I}{da} = -\frac{3h^3 E_{11} \delta_{DCB}^2}{4a^5}. \quad (24)$$

Carlsson et al. (1986) investigated the stability of the ENF specimen, they obtained the following equation:

$$\frac{dG_{II}}{da} = \frac{9\delta_{ENF}^2 a}{8b^2 h^3 E_{11} C_{ENF}^2} \left( 1 - \frac{9a^3}{2L^3 + 3a^3} \right), \quad (25)$$

where  $C_{ENF}$  is the compliance of the ENF specimen:

$$C_{ENF} = \frac{2L^3 + 3a^3}{8b^2 h^3 E_{11}}. \quad (26)$$

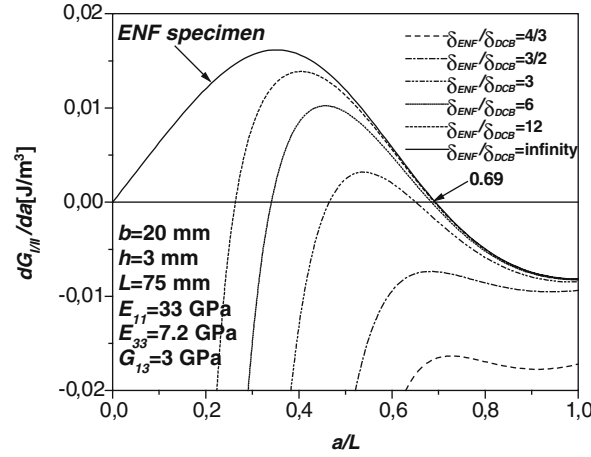


Figure 3. Crack stability chart of the PENF specimen.

The sum of Equations (24) and (25) is:

$$\frac{dG_{I/II}}{da} = \frac{9\delta_{ENF}^2 a}{8b^2 h^3 E_{11} C_{ENF}^2} \left( 1 - \frac{9a^3}{2L^3 + 3a^3} \right) - \frac{3h^3 E_{11} \delta_{DCB}^2}{4a^5} \leq 0. \quad (27)$$

The solution of Equation (27) for different cases is demonstrated in Figure 3. The instability of the system subsequently decays as the crack opening of the PENF specimen increases.

### 3. Experiments

#### 3.1. SPECIMEN MANUFACTURING, MATERIAL AND GEOMETRICAL PROPERTIES

The constituent materials of the E-glass/polyester material used in the present study were procured from Novia Ltd. The properties of the E-glass fiber are  $E = 70$  GPa and  $\nu = 0.27$ , while for the unsaturated polyester resin are  $E = 3.5$  GPa and  $\nu = 0.35$ . Both were considered isotropic. The unidirectional ( $[0^\circ]_{14}$ ) E-glass/polyester specimens with nominal thickness of  $2h = 6.1$  mm, width of  $b = 20$  mm, and fiber-volume fraction of  $V_f = 43\%$  were manufactured in a special pressure tool. A polyamide (PA) insert with thickness of 0.03 mm was placed at the midplane of the specimens to make an artificial starting defect. A great advantage of the present E-glass/polyester material is the transparency, which allows of the visual observation of crack initiation/propagation. The tool was left on room temperature until the specimens became dry. Then the specimens were removed from the tool and were further left on room temperature until 4–6 h. The specimens were cut to the desired length and were pre-cracked in opening mode of 4–5 mm by using a sharp blade. The reason for that was in this case it was possible to make a straight crack front, which is important in the case of the crack length measurement and the observation of the crack initiation. On the other hand, mode-II precracking can be achieved using, e.g. a three-point bending setup; however in this way the crack front would be non-uniform. The flexural modulus was determined from a three-point bending test with span length of

$2L = 150$  mm using six uncracked specimens. The experiment resulted in  $E_{11} = 33$  GPa, additional properties were predicted by using simple rule of mixture, in this way  $E_{33} = 7.2$  GPa,  $G_{13} = 3$  GPa and  $\nu_{13} = 0.27$  were obtained. Three types of tests were performed: the traditional DCB test for pure mode-I, the ENF test for pure mode-II and the mixed-mode I/II PENF test.

### 3.2. DEFINITION OF CRACK INITIATION

The crack initiation was identified visually, i.e. crack initiation was identified when the first non-uniformity concerning the straight crack front was observed.

The accurate determination of the crack length seems to be a difficult issue in the case of carbon or graphite reinforced composites, where the material is not transparent. In general in these cases the change of the crack length is measured by painting the sides of the specimen with white ink (e.g., Morais et al., 2002; Tracy et al., 2003). This should be mentioned that the crack initiates first at the center of the specimen and the crack front is curved. This fact indicates that at the present stage the PENF specimen is recommended mainly for the testing of transparent materials.

### 3.3. DOUBLE-CANTILEVER BEAM TEST

For the DCB test (Figure 1b) four specimens with  $a = 55$  mm were prepared. Steel hinges were bonded to the surfaces of the specimens. The specimens were tested using an Amsler testing machine and were loaded until the point of fracture initiation. At this point the critical crack opening displacement (COD) and the critical load were recorded. The displacement was measured using a mechanical dial gauge, while the values of the applied load were read from the scale of the testing machine.

### 3.4. END-NOTCHED FLEXURE TEST

Similarly, four ENF coupons with initial crack length of  $a = 55$  mm were prepared. The coupons were placed in a three-point bending setup with span length of  $2L = 150$  mm and were loaded up to fracture initiation in the same Amsler testing machine. At this point the critical load and displacement were recorded in a similar fashion to that mentioned in the DCB test.

### 3.5. PRESTRESSED END-NOTCHED FLEXURE TEST

The experimental equipment for the PENF test is demonstrated in Figure 4. The tests were carried out using an Amsler testing machine under displacement control. The span length was  $2L = 150$  mm, the crack length of interest was  $a = 55$  mm. The reason for the latter was that the critical crack opening measured from the DCB test is about 4.5 mm (if  $a = 55$  mm) and the crack tip is far enough (20 mm) from the point of load application. The stiffness, the compliance and the mode-II SERR of the PENF specimen are identical to those of the ENF specimen. We applied six steel rollers to control the mode-I part of the SERR including the following diameters:  $d_0 = 1, 1.5, 2, 2.4, 3$  and 4 mm. It was assumed that the crack opening displacements ( $\delta_{DCB}$ ) in Equations (8) and (20) are equal to these values. To compensate the height

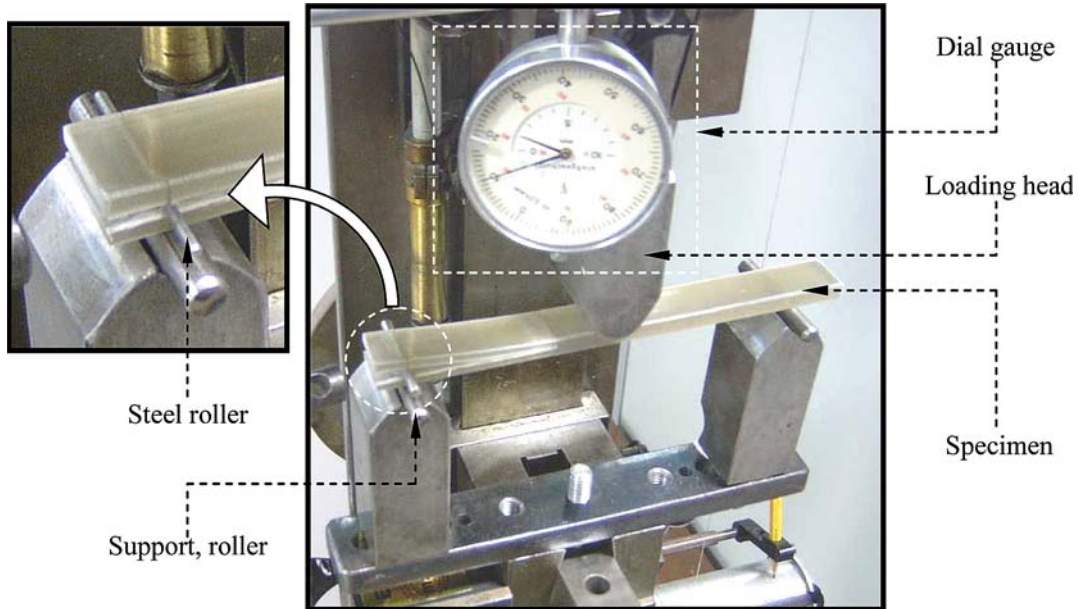


Figure 4. The mixed-mode I/II Prestressed End-Notched Flexure (PENF) specimen.

difference caused by the steel rollers, several underlays with corresponding thicknesses were inserted under the right support in order to hold the specimen in the horizontal plane. It should be mentioned that due to the curved shape of the deflections of the upper and lower specimen arms the contact points between the roller and the arms are slightly shifted. However, due to the relatively small crack opening this was estimated to be very small. Also, due to the relatively high pressure on the rollers caused by the specimen arms the position of the rollers was always stable and no slip occurred. Similarly to the DCB and ENF tests, we applied four coupons at each steel roller. The load–deflection data was measured by using the scale of the testing machine and the dial gauge (see Figure 4).

#### 4. Results and discussion

##### 4.1. LOAD AND DISPLACEMENT

The measured load/displacement traces are shown in Figures 5 and 6. For both cases the response was approximately linear elastic. In fact a very small nonlinearity was observed at the end of the curves, shown in Figures 5a and 6a, however this was not enough to identify the crack initiation without the photographs. At each steel roller four specimens were tested, one of them was used to follow the changes in the straight crack front by making photographs. All the other three specimens were loaded continuously and the crack initiation was observed in situ. So, the former specimen was loaded subsequently, at some points the specimen was relieved, removed from the test rig and the crack front was checked. If the first non-uniformity was observed, then it was considered to be the point of fracture initiation. Figure 5 shows this process in the case of the ENF specimen. The third photo on the crack

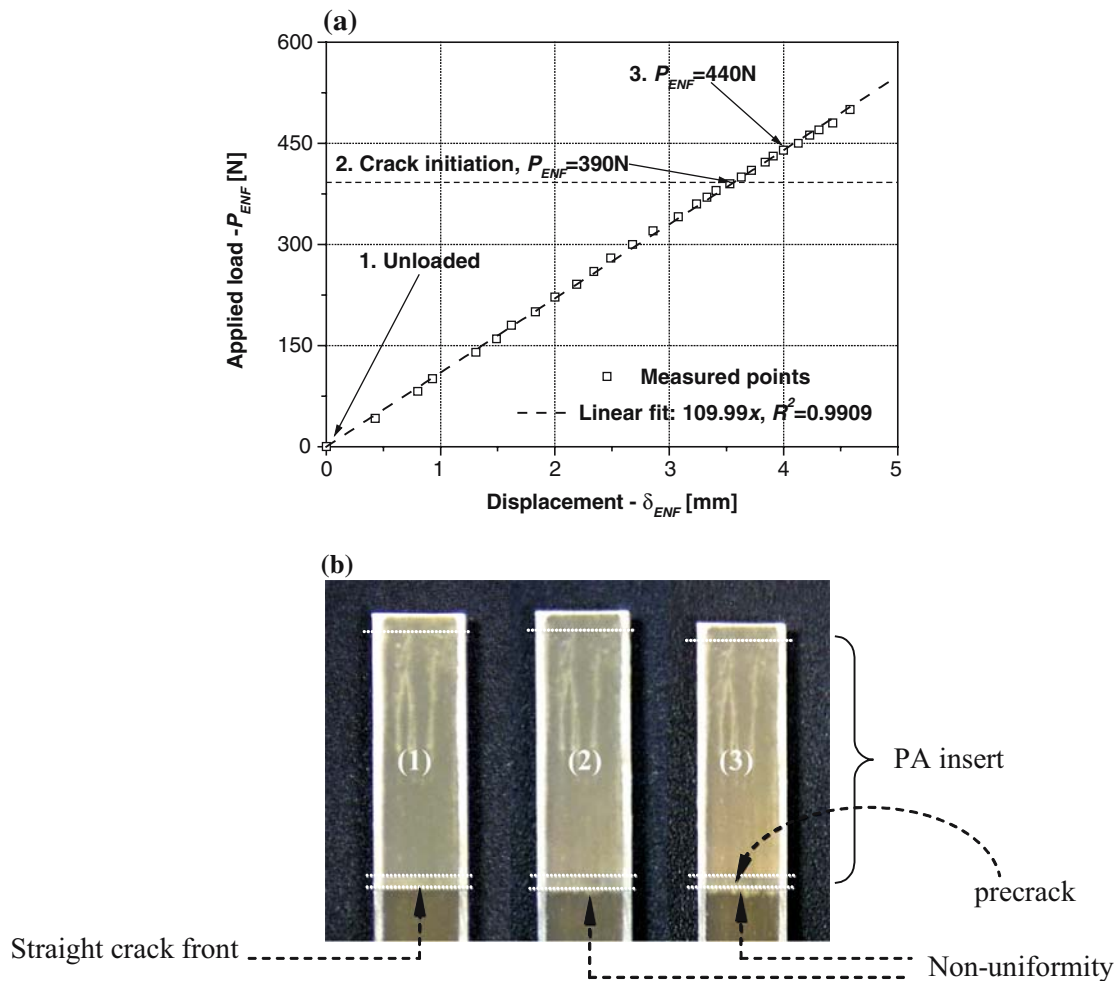


Figure 5. Load–displacement curve of the ENF specimen, ( $d_0=0$  mm) (a), non-uniformity of the crack front at the point of crack initiation (b).

front (Figure 5b) is a typical mode-II crack. The crack initiation process was similar in the case of the PENF specimens, as it is demonstrated in Figure 6.

The load/displacement curves were fit with a linear function, and it was found that they are very close to each other (see the legends in Figures 5a and 6a). As a consequence, the application of steel rollers does not influence the stiffness of the system and the compliance of the PENF system is equal to that of the ENF one.

#### 4.2. DATA REDUCTION

Four techniques were applied to reduce the experimentally measured data. These are given below.

##### 4.2.1. Simple beam theory

*Double-cantilever beam.* The definition  $M_1 = P_1 \cdot a$  was substituted into Equation (1), where  $P_1$  is the value of the load at crack initiation in the DCB specimen.

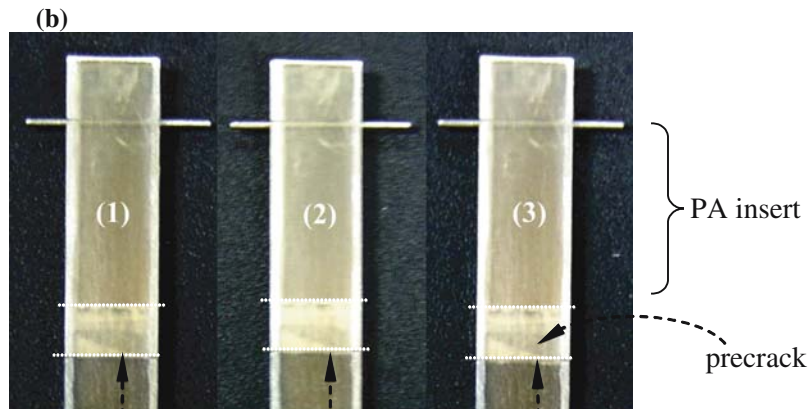
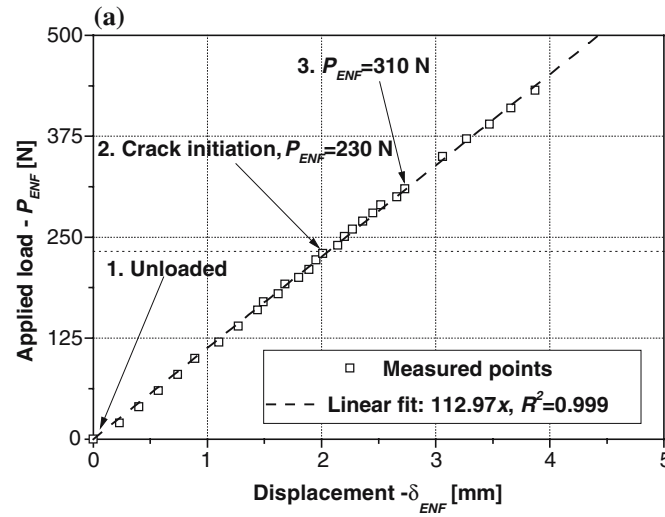


Figure 6. Load–displacement curve of the PENF specimen,  $d_0=2$  mm (a), non-uniformity of the crack front at the point of crack initiation (b).

*End-notched flexure specimen.* For the ENF specimen Equation (9) was used and  $P_{ENF}$  was replaced with  $P_{II}$ , where  $P_{II}$  is the value of the load at crack initiation in the ENF specimen.

*Prestressed end-notched flexure specimen.* For the PENF specimen the energy release rates are given by Equations (8) and (9).

Although the application of the beam theory as a data reduction scheme is simple, in general the accuracy of the method is not satisfactory, because several additional effects are not accounted for (see, e.g., Olsson, 1992; Wang and Qiao, 2004).

#### 4.2.2. Improved beam theory

*Double-cantilever beam.* The definition  $M_I = P_I \cdot a$  was substituted into Equation (11), where  $P_I$  is the value of the load at crack initiation in the DCB specimen.

*End-notched flexure specimen.* Using Equation (21) and replacing  $P_{ENF}$  with  $P_{II}$  gives the improved energy release rate of the ENF specimen, where  $P_{II}$  is the value of the load at crack initiation in the ENF specimen

*Prestressed end-notched flexure specimen.* The improved expressions of the modes I and II energy release rates are given by Equations (20) and (21).

It is noteworthy that in general the additional material properties ( $E_{33}$  and  $G_{13}$ ) are not known with the desired accuracy, because the different rules of mixture give only approximate results. So, the results of the improved expressions (Equations (20)–(22)) should be considered in the light of these establishments.

#### 4.2.3. Direct beam theory

*Double-cantilever beam.* The mode-I energy release rate of the DCB specimen is (Morais et al., 2002):

$$G_{I,DCB}^{DBT} = \frac{3P_I\delta_I}{2ba}, \quad (28)$$

where  $P_I$  and  $\delta_I$  are the load and displacement values at crack initiation in the DCB specimen.

*End-notched flexure specimen.* The direct beam theory (DBT) results in the following formula for the SERR of the ENF specimen (Schön et al., 2000):

$$G_{II,ENF}^{DBT} = \frac{9P_{II}\delta_{II}a^2}{2b(3a^3 + L^3)}, \quad (29)$$

where  $P_{II}$  is the applied load,  $\delta_{II}$  is the displacement of the specimen at the point of load application if crack initiation occurs.

*Prestressed end-notched flexure specimen.* For the application of the direct beam theory the slope of the  $P_I - \delta_I$  curve at  $a = 55$  mm measured from the DCB test was determined averaging the results of four specimens, then the data was fit with a linear function, which resulted in:

$$P_{DCB} = 13.84 \cdot \delta_{DCB}. \quad (30)$$

In the PENF test Equation (30) was used to calculate the load caused by the steel rollers including all the six values of the roller's diameter. The mode-I energy release rate then was calculated using:

$$G_{I,PENF}^{DBT} = \frac{3P_{DCB}\delta_{DCB}}{2ba}. \quad (31)$$

Furthermore, the mode-II component was determined based on Equation (29) by using the measured load and displacement values at the point of load application:

$$G_{II,PENF}^{DBT} = \frac{9P_{ENF}\delta_{ENF}a^2}{2b(3a^3 + L^3)}. \quad (32)$$

According to the DBT the mode-II energy release rate can be obtained directly from the measured load and displacement values of the PENF specimen by using Equation (32). Since the applied load does not cause crack opening we may assume that the complete load is related to the mode-II SERR.

This method has similar drawbacks to the simple beam theory (SBT); however this is the simplest direct data reduction technique, because only one expression determines the energy release rate.

#### 4.2.4. Compliance calibration

*Double-cantilever beam.* For the DCB test 20 specimens were prepared with crack lengths of  $a=20, 25, 30, 35, 40, 45, 50, 55, 60, 65, 70, 75, 80, 90, 100, 110, 120, 130, 140$  and  $150$  mm in order to determine the compliance of the DCB system in a quite extended crack length range. Each specimen was loaded until fracture initiation. The measured data was fit by the following function (Ozdil and Carlsson, 1999a):

$$C_{\text{DCB}} = \beta a^n, \quad (33)$$

where  $\beta$  and  $n$  may be found by using a curve-fit technique. The mode-I energy release rate at the point of crack initiation was determined by the help of the Irwin–Kies expression (e.g., Olsson, 1992) using the same specimens that were used in developing Equation (33):

$$G_{\text{I,DCB}}^{\text{CC}} = \frac{P_{\text{I}}^2}{2b} \frac{dC_{\text{DCB}}}{da}. \quad (34)$$

*End-notched flexure specimen.* For the ENF test 10 specimens were used to determine the compliance curve of the system in the crack length range of  $a=25$  to  $70$  mm with  $5$  mm increments. Each specimen was loaded until fracture initiation occurred. The compliance at each crack length was calculated and the values were fit by a third order polynomial of the form (Schuecker and Davidson, 2000):

$$C_{\text{ENF}} = C_{01} + ma^3, \quad (35)$$

where  $C_{01}$  and  $m$  were found by using least square fitting. In this case the mode-II SERR is:

$$G_{\text{II,ENF}}^{\text{CC}} = \frac{P_{\text{II}}^2}{2b} \frac{dC_{\text{ENF}}}{da}. \quad (36)$$

Again, the SERR was determined for the same specimens that were used for obtaining the  $C(a)$  curve (Equation (35)).

*Prestressed end-notched flexure specimen.* The modes I and II energy release rates were determined by combining the results of the DCB and ENF tests. Using the derivative of the DCB compliance curve (Equation (33)) the mode-I energy release rate is:

$$G_{\text{I,PENF}}^{\text{CC}} = \frac{P_{\text{DCB}}^2}{2b} \frac{dC_{\text{DCB}}}{da}, \quad (37)$$

where  $P_{\text{DCB}}$  was obtained by the help of Equation (30). In a similar fashion, the mode-II component by using the derivative of the ENF compliance curve (Equation (35)) is:

$$G_{\text{II,PENF}}^{\text{CC}} = \frac{P_{\text{ENF}}^2}{2b} \frac{dC_{\text{ENF}}}{da}. \quad (38)$$

It is noteworthy that the application of the CC method is complicated in the case of the PENF specimen. The reason for that is it is not possible to test at a single mode ratio without performing DCB and ENF tests. Furthermore, it is recommended to determine the compliances in a quite extended range of crack length, because

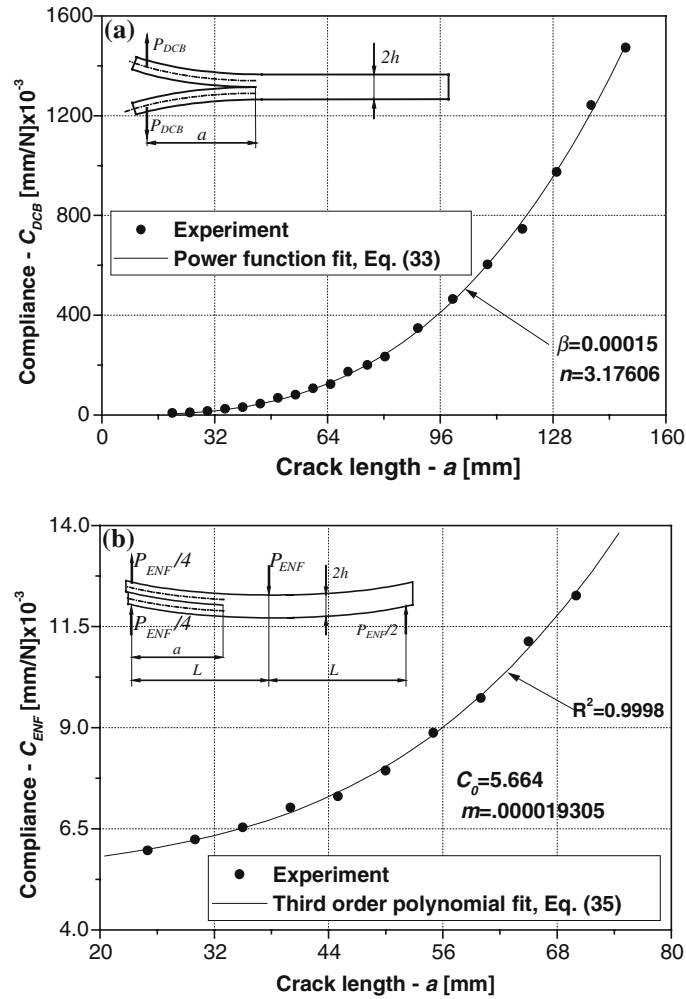


Figure 7. The measured compliance values and the fit compliance curves of the DCB (a) and ENF (b) specimens.

the accuracy of the method depends on the number of points used for the curve-fit process. On the other hand the specimen-to-specimen variation is not accounted for; this may cause problems if the specimens are fabricated using more than one composite plate. The latter problem was eliminated by using the pressure tool (refer to Section 3.1), in which the accuracy of the specimens (concerning the same fiber content and the geometry) is guaranteed.

Figure 7 demonstrates the measured compliance values and the fit curves of the DCB (Figure 7a) and ENF (Figure 7b) systems. Both fit well the measured data. It is remarkable that the exponent ( $n$ ) in Equation (33) was higher than 3.

#### 4.3. CRITICAL ENERGY RELEASE RATES

Table 2 lists the mode mix, the modes I and II and the mixed-mode I/II energy release rates at crack initiation as obtained by the various data reduction schemes.

Table 2. Critical energy release rates calculated by four reduction schemes.

	$\delta_{DCB}$ (mm)	0(ENF)	1	1.5	2	2.4	3	4	4.51(DCB)
Simple beam theory (SBT)	$G_I/G_{II}$	0	0.04	0.13	0.34	0.66	1.64	9.47	$\infty$
		–	$\pm 9e-4$	$\pm 7e-4$	$\pm 6e-3$	$\pm 0.03$	$\pm 0.05$	$\pm 0.52$	–
	$G_I$ (J/m <sup>2</sup> )	0	19.2	43.2	76.7	110.5	172.7	306.9	390.2
	$G_{II}$ (J/m <sup>2</sup> )	741.0	536.2	321.6	229.0	165.9	104.8	33.0	0
		$\pm 18.0$	$\pm 13.8$	$\pm 16.6$	$\pm 3.9$	$\pm 7.6$	$\pm 3.2$	$\pm 1.8$	–
	$G_{I/II}$ (J/m <sup>2</sup> )	741.0	555.4	364.8	305.7	276.4	277.5	339.9	390.2
Improved beam theory (IBT)	$G_I/G_{II}$	0	0.02	0.09	0.22	0.43	1.05	6.09	$\infty$
		–	$\pm 7e-4$	$\pm 4e-3$	$\pm 4e-4$	$\pm 0.02$	$\pm 0.04$	$\pm 0.4$	–
	$G_I$ (J/m <sup>2</sup> )	0	12.8	28.9	51.3	73.9	115.4	205.2	260.9
	$G_{II}$ (J/m <sup>2</sup> )	770.8	553.9	334.1	238.2	173.5	109.6	33.7	0
		$\pm 18.8$	$\pm 16.6$	$\pm 17.3$	$\pm 4$	$\pm 8.2$	$\pm 3.6$	$\pm 2.3$	–
	$G_{I/II}$ (J/m <sup>2</sup> )	770.8	566.7	363.0	289.5	247.4	225.0	238.9	260.9
Direct beam theory (DBT)	$G_I/G_{II}$	0	0.04	0.14	0.34	0.66	1.63	9.19	$\infty$
		–	$\pm 1e-3$	$\pm 6e-3$	$\pm 4e-3$	$\pm 0.03$	$\pm 0.06$	$\pm 0.81$	–
	$G_I$ (J/m <sup>2</sup> )	0	19.3	43.3	77.0	110.9	173.3	308.1	391.7
	$G_{II}$ (J/m <sup>2</sup> )	724.1	522.0	315.4	224.7	165.4	105.0	34.7	0
		$\pm 16.9$	$\pm 18.2$	$\pm 13.2$	$\pm 2.6$	$\pm 7.5$	$\pm 4.0$	$\pm 3.2$	–
	$G_{I/II}$ (J/m <sup>2</sup> )	724.1	541.3	358.7	301.7	276.3	278.3	342.8	391.7
Compliance calibration (CC)	$G_I/G_{II}$	0	0.03	0.10	0.26	0.50	1.25	7.26	$\infty$
		–	$\pm 8e-4$	$\pm 5e-3$	$\pm 4e-3$	$\pm 0.03$	$\pm 0.04$	$\pm 0.5$	–
	$G_I$ (J/m <sup>2</sup> )	0	13.8	31.1	55.3	79.7	124.5	221.4	281.5
	$G_{II}$ (J/m <sup>2</sup> )	700.1	503.2	303.5	216.3	157.6	99.6	30.6	0
		$\pm 17.0$	$\pm 15.0$	$\pm 15.7$	$\pm 3.7$	$\pm 7.4$	$\pm 3.3$	$\pm 2.0$	–
	$G_{I/II}$ (J/m <sup>2</sup> )	700.1	517.0	334.6	271.6	237.3	224.1	252.0	281.5
IBT ( $G_I$ ) DBT( $G_{II}$ )	$G_I/G_{II}$	0	0.025	0.09	0.23	0.45	1.10	5.91	$\infty$
		–	$\pm 9e-4$	$\pm 4e-4$	$\pm 3e-3$	$\pm 0.03$	$\pm 0.04$	$\pm 0.54$	–
	$G_I$ (J/m <sup>2</sup> )	0	12.8	28.9	51.3	73.9	115.4	205.2	260.9
	$G_{II}$ (J/m <sup>2</sup> )	724.1	522.0	315.4	224.7	165.4	105.0	34.7	0
		$\pm 16.9$	$\pm 18.2$	$\pm 13.2$	$\pm 2.6$	$\pm 7.5$	$\pm 4.0$	$\pm 3.2$	–
	$G_{I/II}$ (J/m <sup>2</sup> )	724.1	534.8	344.2	276.0	239.3	220.5	239.9	260.9

The geometries tested had properties of  $a = 55$  mm and  $2L = 150$  mm and at each steel roller four coupons were used. The scatter is also given in the case of the mode ratio and the mode-II component. Since the mode-I SERR is fixed; the scatter of  $G_{I/II}$  is equal to that of the  $G_{II}$ . From Table 2 one can see that the complete range of mode-mixity can be covered using the PENF coupon.

The mode-I critical SERR is somewhat higher in accordance with the simple beam theory compared to the result by improved beam theory. The reason for that is IBT

accounts for crack tip deformation and rotation, and therefore predicts a slightly lower force caused by the steel roller. This fact results in a lower mode-I SERR. In contrast, the improved beam theory predicts a higher critical mode-II SERR compared to the simple beam model, which can be explained by the fact that the former takes the crack tip shear deformation (Wang and Qiao, 2004; Szekrényes and Uj, 2005) into account. The results of the experimental reduction techniques are shown in the third and fourth blocks of Table 2. It is shown that the results calculated by DBT are very similar to those calculated by simple beam theory (first block of Table 2). As it was mentioned in Section 4.2, these methods have similar deficiencies. Finally, the results of the compliance calibration correspond well with those calculated by the improved beam theory. This conclusion confirms the application of the improved expressions (Equations (20)–(22)), and it seems that the way in which the additional material properties were determined is acceptable.

Seeing the results of Table 2 it transpires that the difference between the  $G_I$  results of the simple and improved beam model (or between the results by the CC method and direct beam theory) increases as the mode ratio increases. On the contrary, the greater the mode ratio the smaller the difference between the values of  $G_{II}$  as obtained by simple and improved beam theory. In spite of the good agreement between the CC method and improved beam theory it should be mentioned that there is an inherent smoothing process that comes into play by using a single CC curve for all specimens. Thus, some caution needs to be employed in generalizing the results and conclusions considering the CC method.

The mixed-mode I/II energy release rate by SBT and IBT agree well if  $\delta_{DCB}$  is 1.5 mm. In this respect the best agreement between the DBT and CC methods is expected if  $\delta_{DCB}$  is between 1 and 1.5 mm.

As a summary, for unidirectional composites the IBT is reliable and simple to apply, as it has been highlighted by other authors (e.g., Ducept et al., 1997; Ozdil and Carlsson, 1999), although the CC method is more reliable in angle-ply laminates. The reason for that is the difference in the predicted and manufactured stiffnesses (Davidson and Sundararaman, 1996). Although one would expect that the CC method yield the most accurate result, this is the most complicated reduction technique due to the large number of DCB and ENF specimens required to data reduction. From Table 2 a comparison of results for total SERR in the DCB and ENF configurations shows that the IBT is the most accurate in mode-I, while the DBT is the most accurate in mode-II compared to the results by the CC method. The accuracy of the IBT is +7.2% in mode II and –7.3% in mode-I compared to the CC technique. Because of the SERR of the DCB and ENF systems was determined using the same specimens used for developing the  $C(a)$  curve, we may assume that its accuracy is within this range also for other mode-mixities. The last block of Table 1 presents the results obtained by using the IBT for mode-I and the DBT for mode-II. This way we obtain the best correlation to the CC method considering the total SERR, while in the case of the mode ratio the values are similar to the results by IBT. The scatter in Table 2 is within reasonable ranges in all the cases, however due to the nature of the CC method (each specimen has the same  $dC/da$ , and so only the scatter of the mode-II component is included) one must be careful about generalizing these results. Thus, the recommended data reduction method is the IBT for mode-I and DBT for mode-II.

#### 4.4. FRACTURE ENVELOPES

The different mixed-mode I/II fracture criteria were reviewed by Reeder (1992), Rikards et al. (1998) and Kim and Mayer (2003). We apply the two most popular criteria. In accordance with the traditional power criterion the following relation may be established between the mode-I and mode-II strain energy release rates (e.g., Hashemi et al., 1990b):

$$\left(\frac{G_I}{G_{IC}}\right)^{p_1} + \left(\frac{G_{II}}{G_{IIC}}\right)^{p_2} = 1, \quad (39)$$

On the other hand Williams' criterion (e.g., Hashemi et al., 1990a, b) recommends the following expression:

$$\left(\frac{G_I}{G_{IC}} - 1\right)\left(\frac{G_{II}}{G_{IIC}} - 1\right) - I_i \left(\frac{G_I}{G_{IC}}\right)\left(\frac{G_{II}}{G_{IIC}}\right) = 0, \quad (40)$$

where  $I_i$  is the interaction parameter between the mode-I and mode-II SERRs. If  $I_i = 0$  then there is no interaction. Also, if  $I_i = 1$  then Equation (40) states a simple addition. In Equations (39) and (40)  $G_{IC}$  is the critical strain energy release rate under pure mode-I (calculated from the data of the DCB specimen),  $G_{IIC}$  is the mode-II critical strain energy release rate (calculated from the data of the ENF specimen). The results of the PENF test (listed in Table 2) were used to provide six additional points in the  $G_I$ - $G_{II}$  plane. The power parameters ( $p_1, p_2$ ) in Equation (39) and the interaction parameter ( $I_i$ ) in Equation (40) were determined by a curve-fit technique.

The calculated fracture envelopes are displayed in Figure 8 calculated by two different schemes: the compliance calibration (Figure 8a) and the combined IBT-DBT method (Figure 8b). It is interesting that the interaction parameter  $I_i$  was the same in both figures; although the differences between the power parameters are also small ones. The mode-I critical SERR is somewhat higher in accordance with the CC method compared to the result by IBT-DBT technique. Figure 8 indicates that there are negligible differences between the CC method and the combined IBT-DBT scheme. Overall, the difference between the power and Williams' criteria is negligible, both describes the same failure locus. However, the application of Williams' method is simpler.

#### 4.5. COMPARISON WITH PUBLISHED RESULTS

For comparison we present the results of similar experiments, which were published in the literature. In the first block of Table 3 the results by Ozdil and Carlsson (1999b) obtained by using MMB specimens are given. The scatter of the data is also included, where it is available. The unidirectional glass/polyester specimens had similar fiber-volume fraction (45%) to that of our coupons. The power parameters are very close to those shown in Figures 8 and 9. The curves of the criteria are rather concave; however, they are close to a linear curve. From other point of view the interaction parameter  $I_i$  is significantly higher in our experiment. This may be explained by the fact that Williams' criterion is not too sensitive to a relatively large change in the interaction parameter.

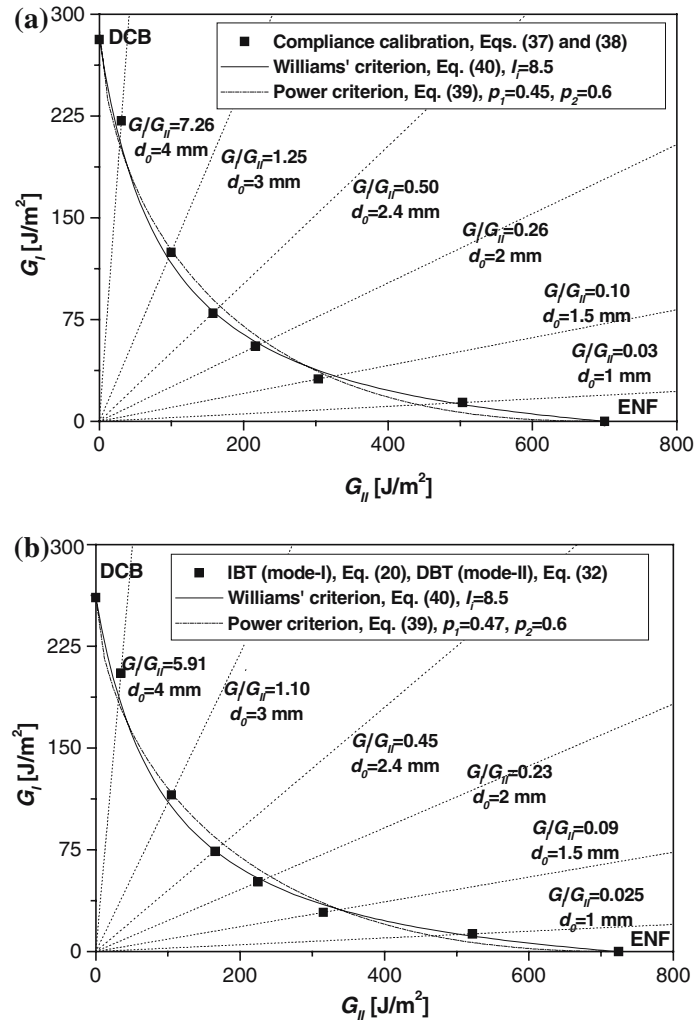


Figure 8. Interlaminar fracture envelopes for glass/polyester composite calculated by using compliance calibration method (a) and the combination of the IBT (mode-I) and DBT (mode-II) methods.

The second block of Table 3 presents the results by Ducept et al. (1999), who also used MMB specimens manufactured from glass/epoxy composite. This time the parameters of the criteria are not given. The reason for that is in this case the application of the two mentioned criteria does not seem to be reasonable. Overall, the shape of the envelope is convex.

Hashemi et al. applied the DCB, ELS and the mixed-mode I/II SCB specimens to determine the failure locus for carbon/PEEK (Hashemi et al., 1990a) and polyether-sulphone fiber (PES) (Hashemi et al., 1990b) composites. In the latter case the SCB coupon was applied including three different mode ratios by varying the thickness ratio of the specimen arms. The third and fourth blocks in Table 3 present the results of these experiments. For the carbon/PEEK material the curve of the envelope is concave, similarity to the results by Ozdil and Carlsson (1999b) may be established. On the contrary, the curve of the failure criterion is convex for the PES composite.

Table 3. Interlaminar fracture toughness values and failure criteria parameters for composite materials.

Ozdil and Carlsson (1999b),MMB, glass/polyester: $E_{11} = 29.1$ GPa, $E_{33} = 8.5$ GPa, $G_{13} = 4.34$ GPa, $\nu_{13} = 0.27$						
$h = 2.19$ mm, $b = 20$ mm	$G_I/G_{II}$	0	0.29	1.03	4.04	$\infty$
$p_1 = 0.78$ , $p_2 = 0.87$ , $I_1 = 1.5$	$G_{I/II}$ (J/m <sup>2</sup> )	$496 \pm 135$	$365 \pm 22$	$311 \pm 45$	$293 \pm 38$	$282 \pm 42$
Ducept, Davies and Gamby (1997), MMB, glass/epoxy: $E_{11} = 25.7$ GPa, $E_{33} = 6.5$ GPa, $G_{13} = 2.5$ GPa, $\nu_{13} = 0.32$						
$h = 2.5$ mm, $b = 20$ mm	$G_I/G_{II}$	0	0.14	0.374	1.112	$\infty$
	$G_{I/II}$ (J/m <sup>2</sup> )	$1530$ (10%)	$1368$ (4.8%)	$1002$ (9.3%)	$674$ (16.5%)	$259$ (6%)
Hashemi et al. (1990a), DCB-ELS-SCB, carbon/PEEK: $E_{11} = 124$ GPa, $E_{33} = 10$ GPa, $G_{13} = 5$ GPa, $\nu_{13} = 0.38$						
$h = 2.65$ mm, $b = 25$ mm	$G_I/G_{II}$	0	1.33	$\infty$		
$p_1 = 0.76$ , $p_2 = 0.83$ , $I_1 = 1.33$	$G_{I/II}$ (J/m <sup>2</sup> )	$1730 \pm 40$	$1530$ (-)	$1800 \pm 15$		
Hashemi et al. (1990b), DCB-ELS-SCB, PES: $E_{11} = 132$ GPa, $E_{33} = 8$ GPa, $G_{13} = 3.5$ GPa						
$h = 2.025$ mm, $b = 20$ mm	$G_I/G_{II}$	0	0.84	1.33	2.13	$\infty$
$p_1 = 1.4$ , $p_2 = 1.8$ , $I_1 = 0.26$	$G_I$ (J/m <sup>2</sup> )	$1250$	$1290$	$1180$	$1100$	$800$

It is obvious that the shape of the fracture envelope (concave, convex or linear) depends on the material applied for testing.

## 5. Conclusions

In this work the prestressed end-notched flexure specimen was developed for interlaminar fracture testing of laminated composite materials. Apart from the traditional DCB and ENF tests the PENF specimen was used to obtain the mixed-mode I/II energy release rate at propagation onset including six different mode ratios. To perform the experiments unidirectional E-glass/polyester specimens were manufactured. The measured data was reduced using four different approximations: simple (Euler–Bernoulli) beam theory, improved beam theory, direct beam theory and the compliance calibration. The simple beam theory was found to be inaccurate for both components of the SERR, while the CC was expected to be the most accurate reduction scheme, however due to its difficulties it did not seem to be the optimal scheme. Based on the results obtained it was found that the best agreement with the results of the CC method can be obtained if we use the improved beam theory for the determination of the mode-I component and the direct beam theory for the calculation of the mode-II component. Thus a combined IBT-DBT scheme is recommended for data evaluation.

The fracture envelope of the present material was determined using two criteria: the power criterion and Williams' criterion. In each case both predicted the same failure locus. The obtained results were compared to results by other authors using different configurations. The differences were attributed to the different materials applied for testing.

The PENF specimen offers several advantages. It requires the simplest specimen geometry and the simplest experimental equipment (three-point bending setup, steel rollers). It was shown that the PENF specimen is able to produce any mode ratio at crack propagation onset and the traditional reduction techniques (CC method, direct beam theory) can be applied for data evaluation. As a consequence the mode-mixity can be determined also experimentally. During the test no large displacements and geometrical nonlinearities were observed. The drawbacks of the PENF specimen are that the mode ratio changes with the crack length and the applied load, so the method is recommended mainly for the testing of transparent composite materials. Finally, the mode ratio can not be calculated without performing experiments, involving the fact that the mode ratio will depend on the definition of the crack initiation and the accuracy of the measurement of the load and crack length.

More work is required to reduce the drawbacks of the test and to make it applicable for non-transparent materials.

## 6. Acknowledgement

This research work was sponsored by the Hungarian Ministry of Education (OM) under Grant No. T30833-066 (41). The author is grateful to Tonny Nyman for providing the references by Williams (1988) and Yoon and Hong (1990a), Alfredo Balacó de Moraes for the reference by Davies et al. (1996), Pizhong Qiao for the paper by Wang and Qiao (2003). I wish also to thank Barry D. Davidson for sending his work (Davidson and Sundararaman, 1996) to me.

## References

- Arcan, M., Hashin, Z. and Voloshin, A. (1978). A method to produce plane-stress states with applications to fiber-reinforced materials. *Exp. Mech.* **18**, 141–146.
- Asp, L.E. (1998). The effects of moisture and temperature on the interlaminar delamination toughness of a carbon/epoxy composite. *Composit. Sci. Technol.* **58**, 967–977.
- ASTM D6671 – 01. (2001). Standard test method for mixed mode I-mode II interlaminar fracture toughness of unidirectional fibre reinforced polymer matrix composites, *Annual Book of ASTM Standards*, Vol. 15.03, 100 Barr Harbor Drive, West Conshohocken, PA 19428, USA.
- Bradley, W.L. and Cohen, R.N. (1985). Matrix deformation and fracture in graphite-reinforced epoxies. In *Delamination and Debonding of Materials* (Edited by Johnson S.W.) American Society for Testing and Materials, Philadelphia, ASTM STP **876**, 389–410.
- Carlsson, L.A., Gillespie, J.W. and Pipes, R.B. (1986). On the analysis and design of the end notched flexure (ENF) specimen for mode II testing. *J. Composit. Mater.* **20**, 594–604.
- Chen, J.H., Sernow, R., Schulz, G. and Hinrichsen, G. (1999). A modification of the mixed-mode bending test apparatus. *Composites Part A: Appl. Sci. Manufact.* **30**, 871–877.
- Chen, L., Sankar B.V. and Ifju P.G. (2003). Mixed-Mode Fracture Toughness Tests for Stitched Composite Laminates. *AIAA Paper 2003–1874*, In *Proceedings of the 44th AIAA Structures, Structural Dynamics and Materials Conference*, Norfolk, Virginia, April 7–10, 2003, 10 p.
- Crews, Jr J.H. and Reeder, J.R. (1988). A mixed-mode bending apparatus for delamination testing. *NASA Technical Memorandum 100662*, August, 1–37.
- Davidson, B.D. and Sundararaman, V. (1996). A single leg bending test for interfacial fracture toughness determination. *Int. J. Fracture* **78**, 193–210.
- Davies, P., Ducept, F., Brunner, A.J., Blackman, B.R.K. and Morais, de A.B. (1996). Development of a standard mode II shear fracture test procedure. In: *Proceedings of the 7th European Conference on Composite Materials (ECCM-7)* Vol. 2, London, May, pp 9–15.
- Davies, P., Casari, P. and Carlsson, L.A. (2005). Influence of fiber volume fraction on the interlaminar fracture toughness of glass/epoxy using the 4ENF specimen. *Composit. Sci. Technol.* **65**, 295–300.
- Ducept, F., Davies, P. and Gamby D. (1997). An experimental study to validate tests used to determine mixed mode failure criteria of glass/epoxy composites. *Composites Part A: Appl. Sci. Manufact.* **28A**, 719–729.
- Ducept, F., Gamby, D. and Davies, P. (1999). A mixed-mode failure criterion derived from tests of symmetric and asymmetric specimens. *Composit. Sci. Technol.* **59**, 609–619.
- Ducept, F., Davies, P. and Gamby, D. (2000). Mixed mode failure criteria for a glass/epoxy composite and an adhesively bonded composite/composite joint. *Int. J. Adhesion and Adhesives* **20**, 233–244.
- Edde, F.C. and Verreman, Y. (1995). Nominally constant strain energy release rate specimen for the study of mode II fracture and fatigue in adhesively bonded joints. *Int. J. Adhesion and Adhesives* **15**, 29–32.
- European Structural Integrity Society (ESIS). (2000). Determination of the mixed-mode I/II delamination resistance of unidirectional fibre-reinforced polymer laminates using the asymmetric double cantilever beam specimen (ADCB). *Polymers and Composites Task Group*, version 00–05–03.
- Hashemi, S., Kinloch, J. and Williams, J.G. (1987). Interlaminar fracture of composite materials. In *Proceedings of the 6th ICCM and ECCM Conference*, Vol. 3, Elsevier Applied Science, London, pp. 3.254–3.264.
- Hashemi, S., Kinloch, J. and Williams, J.G. (1990a). The effects of geometry, rate and temperature on mode I, mode II and mixed-mode I/II interlaminar fracture toughness of carbon-fibre/poly(ether-ether ketone) composites. *J. Composit. Mater.* **24**, 918–956.
- Hashemi, S., Kinloch, J. and Williams, J.G. (1990b). Mechanics and mechanisms of delamination in a poly(ether sulphone)-fibre composite. *Composit. Sci. Technol.* **37**, 429–462.
- Ifju, P.G., Chen, L.-S. and Sankar, B.V. (2002). Mixed-mode fracture toughness for stitched composites. SEM Annual Conference, Milwaukee, WI 2002, paper number 173.
- Kim, B.W. and Mayer, A.H. (2003). Influence of fiber direction and mixed-mode ratio on delamination fracture toughness of carbon/epoxy laminates. *Composit. Sci. Technol.* **63**, 695–713.
- Korjakin, A., Rikards, R., Buchholz, F.-G., Wang, H., Bledzki, A.K. and Kessler, A. (1998). Comparative study of interlaminar fracture toughness of GFRP with different fiber surface treatments. *Polymer Composites* **19**, 793–806.

- Lai, Y.-H., Rakestraw, M.D. and Dillard, D.A. (1996). The cracked lap shear specimen revisited – a closed form solution. *Int. J. Solids and Struct.* **33**, 1725–1743.
- Morais, de A.B., Moura, de M.F., Marques, A.T. and Castro, de P.T. (2002). Mode-I interlaminar fracture of carbon/epoxy cross-ply composites. *Composit. Sci. Technol.* **62**, 679–686.
- Olsson, R. (1992). A simplified improved beam analysis of the DCB specimen. *Composit. Sci. Technol.* **43**, 329–338.
- Ozdil, F., Carlsson, L.A. and Davies, P. (1998). Beam analysis of angle-ply laminate end-notched flexure specimens. *Composit. Sci. Technol.* **58**, 1929–1938.
- Ozdil, F. and Carlsson, L.A. (1999a). Beam analysis of angle-ply laminate DCB specimens. *Composit. Sci. Technol.* **59**, 305–315.
- Ozdil, F. and Carlsson, L.A. (1999b). Beam analysis of angle-ply laminate mixed-mode bending specimens. *Composit. Sci. Technol.* **59**, 937–945.
- Qiao, P., Wang, J. and Davalos, J.F. (2003b). Analysis of tapered ENF specimen and characterization of bonded interface fracture under mode-II loading. *Int. J. Solids Struct.* **40**, 1865–1884.
- Raju, I.S., Crews, Jr J.H. and Aminpour, M.A. (1988). Convergence and strain energy release rate components for edge-delaminated composite laminates. *Eng. Fracture Mech.* **30**, 383–396.
- Reeder, J.R. and Crews, Jr J.H. (1990). Mixed-mode bending method for delamination testing. *AIAA J* **28**, 1270–1276.
- Reeder, J.R. and Crews, Jr J.H. (1991). Nonlinear analysis and redesign of the mixed-mode bending delamination test. *NASA Tech. Memorandum 102777*, January, 1–49.
- Reeder, J.R. (1992). An evaluation of mixed-mode delamination failure criterion. *NASA Technical Memorandum 104210*, February, 1–49.
- Reeder, J.R. (2000). Refinements to the mixed-mode bending test for delamination toughness. *NASA-2000-ASC15ATC*; 1–8.
- Rhee, K.Y. and Chi, C.H. (2001). Determination of fracture toughness,  $G_C$  of Graphite/epoxy composites from a cracked lap shear (CLS) specimen. *J. Composit. Materi* **35**, 77–93.
- Rikards, R., Buchholz, F.G., Wang, H., Bledzki, A.K., Korjakin, A. and Richard H.-A. (1998). Investigation of mixed mode I/II interlaminar fracture toughness of laminated composites by using a CTS type specimen. *Eng. Fracture Mech.* **61**, 325–342.
- Schön, J., Nyman, T., Blom, A. and Ansell, H. (2000). Numerical and experimental investigation of a composite ENF-specimen. *Eng. Fracture Mech.* **65**, 405–433.
- Schuecker, C. and Davidson, B.D. (2000). Evaluation of the accuracy of the four-point bend end-notched flexure test for mode II delamination toughness determination. *Composit. Sci. Technol.* **60**, 2137–2146.
- Sørensen, B.F., Jørgensen, K., Jacobsen, T.K. and Østergaard, R.C. (2004). A general mixed-mode fracture specimen: The DCB specimen loaded with uneven bending moments. *Print. Pitney Bowes Management Services A/S - Risø-R-1394(EN)*, 1–35.
- Sundararaman, V. and Davidson, B.D. (1997). An unsymmetric double cantilever beam test for interfacial fracture toughness determination. *Int. J. Solids and Struct.* **34**, 799–817.
- Sundararaman, V. and Davidson, B.D. (1998). An unsymmetric end-notched flexure test for interfacial fracture toughness determination. *Eng. Fracture Mech.* **60**, 361–377.
- Szekrényes, A. and Uj, J. (2004). Beam and finite element analysis of quasi-unidirectional SLB and ELS specimens. *Composit. Sci. Technol.* **64**, 2393–2406.
- Szekrényes, A. (2005). Delamination of composite specimens. *PhD Thesis*, Budapest University of Technology and Economics, Faculty of Mechanical Engineering, Department of Applied Mechanics, Budapest, PhD-261/2004.
- Szekrényes, A. and Uj, J. (2005). Mode-II fracture in E-glass/polyester composite. *J. Composit. Materi.* **39**, 1747–1768.
- Szekrényes, A. and Uj, J. (2006a). Comparison of some improved solutions for mixed-mode composite delamination coupons. *Composit. Struct.* **72**, 321–329.
- Szekrényes, A. and Uj, J. (2006b). Over-leg bending test for mixed-mode I/II interlaminar fracture in composite laminates. *Int. J. Damage Mech.* (accepted for publication).
- Tracy, G.D., Feraboli, P. and Kedward, K.T. (2003). A new mixed mode test for carbon/epoxy composite systems. *Composites Part A: Appl. Sci. Manufact.* **34**, 1125–1131.
- Wang, J. and Qiao, P. (2003). Fracture toughness of wood-wood and wood-FRP bonded interfaces under mode-II loading. *J. Composit. Materi.* **37**, 875–898.

- Wang, J and Qiao, P. (2004). Novel beam analysis of the end notched flexure specimen for mode-II fracture. *Eng. Fracture Mech.* **71**, 219–231.
- Wang, H. and Vu-Khanh, T. (1996). Use of end-loaded-split (ELS) test to study stable fracture behaviour of composites under mode-II loading. *Composit. Struct.* **36**, 71–79.
- Wang, W.-X., Takao, Y. and Nakata, M. (2003). Effects of friction on the measurement of the mode II interlaminar fracture toughness of composite laminates. In: *Proceedings of the 14th International Conference on Composite Materials* (CD-ROM), Manuscript No.:1429, July 14–18, San Diego, California, USA.
- Wang, Y. and Williams, J.G. (1992). Corrections for mode II fracture toughness specimens of composite materials. *Composit. Sci. Technol.* **43**, 251–256.
- Williams, J.G. (1988). On the calculation of energy release rates for cracked laminates. *Int. J. Fracture* **36**, 101–119.
- Williams, J.G. (1989). End corrections for orthotropic DCB specimens. *Composit. Sci. Technol.* **35**, 367–376.
- Yoon, S.H. and Hong, C.S. (1990a). Modified end notched flexure specimen for mixed mode interlaminar fracture in laminated composites. *Int. J. Fracture* **43**, R3–R9.
- Yoon, S.H. and Hong, C.S. (1990b). Interlaminar fracture toughness of graphite/epoxy composite under mixed-mode deformations. *Exp. Mech.* **30**, 234–239.